Nozzle-internal particle velocity measurements and loading effect on particle acceleration inside a Cold Spray nozzle

M. Meyer, F. Caruso, *R. Lupoi, Trinity College Dublin, The University of Dublin, Department of Mechanical and Manufacturing Engineering, Parsons Building, Dublin 2, Ireland *Contact email: lupoir@tcd.ie

The advantages of the solid state deposition process Cold Spray (CS) over conventional spray technologies go hand in hand with the requirement of high and well-predictable particle velocities. The acceleration of particles primarily takes place within the CS-nozzle while measurements of their velocity are conducted downstream of its exit. Despite their essential value, these observations are limited, in that only the result of the acceleration can be evaluated, not the actual driving mechanisms themselves. Previous work has indicated that there is no conclusive understanding of these mechanisms, especially in cases of increasing particle loading. This study therefore presents a transparent rectangular CS-nozzle design (made out of quartz) for a low stagnation pressure regime. A novelty to the field of thermal spray is the first report of particle in-flight measurements within the CS-nozzle using Particle Tracking Velocimetry (PTV) at varying particle loadings and pressure levels. It is found that particle velocities in the jet decrease with increasing particulate loading as the momentum exchange of the gas is enhanced, while in the subsonic flow region, the average velocity level increases due to particle-particle interactions with shallower axial velocity profiles. This effect is aggravated for higher working pressures, as energetic collisions cause increasing losses, depending on the number density of particles. This study forms the basis for a comprehensive nozzle-internal analysis.

1 Introduction

The coating manufacturing process Cold Spray (CS) makes use of high speed impact and deposition of particles from a feedstock powder onto a substrate. The impact velocities are obtained from a driving process gas flow through a supersonic nozzle, which enables very low temperature levels compared to other coating technologies and therefore a solid state deposition. This minimizes disadvantages of melting and hence provides a possibility to coat oxidisation-sensitive materials and material combinations with different melting temperatures [1][2] opening a wide field of interesting applications. For deposition to succeed, a material-specific critical impact velocity must be crossed, which makes the particle acceleration a critical aspect of the technology [3][4]. Both experimental and numerical studies on the particle-laden gas nozzle flow were conducted in the past decades, identifying the main parameters for particulate acceleration. Primarily, the gas stagnation pressure and temperature [5][6], the gas species [7][8], powder injection conditions [9][10] and particle material and size [11][12][13], as well as shape [14][15] are important. An important part of this progress was the use of optical measurement techniques: Schlieren photography was frequently used to visualise flow features of the gas phase. The quantification of the velocity and particle motion however required other, non-intrusive velocity measurement techniques, of which several were employed over the years: laser-two-focus (L2F) [16], doppler picture velocimetry (DVP) [17], and lastly Particle image velocimetry (PIV) or similar techniques, in particular Particle Tracking Velocimetry (PTV). The latter techniques could be used to record instantaneous particle velocity distributions throughout the field of measurement [18][19][20]. Depending on the particle feed rate and the relative gas consumption, the discrete phase loading can increasingly affect the acceleration process. Although Pardhasaradhi et al. [21] found that the effect is negligible at low mass fractions of the discrete phase, results demonstrated by Samareh et al. [22] indicated that the gas flow structures change and the particle speed reduces as the particle mass fraction increases. With respect to engineering applications, a study by Lupoi [23] showed that a series of experimental observations could not be explained by computational techniques that ignore phase coupling effects, which were improved by Meyer & Lupoi [24] when inter-phase momentum-exchange was included. The authors also published a validation case of most prevalent computational techniques with attention to this aspect [25], stating that the models can reproduce the trend of decreasing velocities with feed rate, nevertheless fail to provide reliable quantitative results, suggesting that neglected effects such as particle-particle interactions and the particle volume fraction in fact contribute noticeably to the particle velocity level. Meyer et al. [26] recently extended their work on the matter by an experimental investigation that begins to identify driving mechanisms for the velocity drop and ties the susceptibility of high-density materials predominantly to mass loading and such of low-density materials rather to volume fraction. It remains unknown what in detail leads to this interplay, and consequently conclusive understanding of the phase coupling effects still has to be achieved.

The benefit of higher particle feed rates is without doubt faster processing times in manufacturing applications. Moreover, a cost analysis of the CS process by Stier [27] provides evidence that it is important to understand the mass loading effect also on an economical level, as it enables the optimisation of gas and powder consumption without loss of deposition efficiency.

The acceleration of particles and the potential causes for coupling effects primarily take place within the CS-nozzle, while the optical measurements to date had to

be conducted downstream of its exit. Despite their essential value, these observations are limited as only the result of the acceleration can be evaluated, not the actual driving mechanisms. Therefore, this work aims to investigate the particle velocity not only in the jet of a CS system, but also within the internal channel of the nozzle itself. A transparent quartz nozzle with rectangular cross-section and a de-Laval shape, characteristic for CS nozzles, was designed for this purpose. PTV was used to measure Stellite-21 particle velocities at varying low stagnation pressure and feeding conditions. This study is the very first attempt of a quantitative measurement of a nozzle-internal flow, and therefore represents a very distinct novelty to the field. Establishing such techniques would not only give insight into the mechanisms of the particle acceleration, but also enable direct studies on the injection process.

2 Methods

2.1 Cold Spray system, nozzle and materials

Fig. 1a) illustrates a schematic of the experimental arrangement, including PIV and the CS process. The nitrogen gas flow was fed from a high pressure gas supply line, regulated to different settings of constant pressure between 3 and 8bar-g at the nozzle inlet. The gas line was split into two lines, a main line, which was connected to the nozzle head, and a powder feeder line, both comprising flow meters and pressure gauges. The wheel type powder feeder was set to varying wheel speeds and included a load cell to measure the mass feed rate of powder. The range of pressure and wheel speed settings can be found in Table 1. Downstream of the powder feeder, the gas–solid mixture then merged with the main flow in the nozzle head with a central injection position. **Fig. 1**b) shows the measurement set-up as arranged in the facilities. Details of the imaging procedure can be found in sections to follow, however the core piece of the setup is the transparent quartz nozzle. An illustration of it is presented in **Fig. 1**c). This in-house nozzle-design has rectangular cross-section in order to provide a wall contour only in one dimension and a flat nozzle wall in the other dimension, through which the image can be recorded. The de-Laval converging/diverging shape had a full length of 150mm and an expansion ratio of 3.72. As the design point for this expansion ratio, a pressure level of 10bar-g was chosen, leading to a slightly over-expanded flow condition under such circumstances. Due to beginning design-related leakage at this pressure, the nozzle operation was limited to 8bar. The low stagnation pressure regime was set as the target because the stability of the nozzle is a limiting factor due to its material. Based on pre-tests, quartz was chosen, since it provides the best possible transparency and the least image distortions, while it is hard enough to withstand erosion at moderate speed levels. As can be seen in **Fig. 1**c), the measurements were conducted in two locations for all settings. Firstly, the low-speed converging section down to the nozzle throat was investigated, since this part is characterised by a relatively large particle number density as compared to the high- speed section and therefore is the most important candidate for regions with strong interactions.

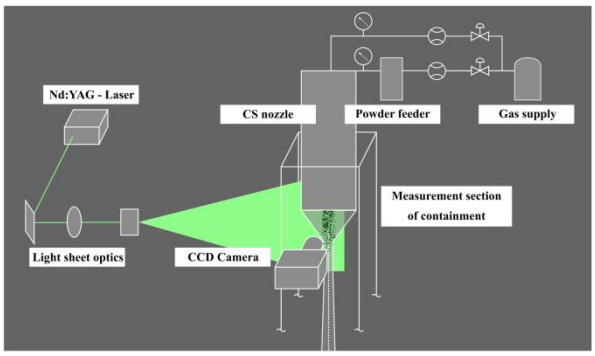

(a) Set-up scheme

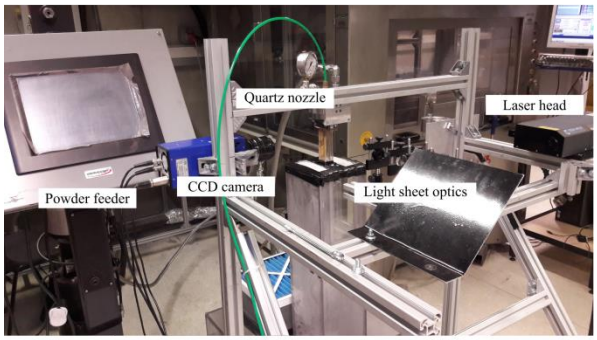

(b) Experimental arrangement

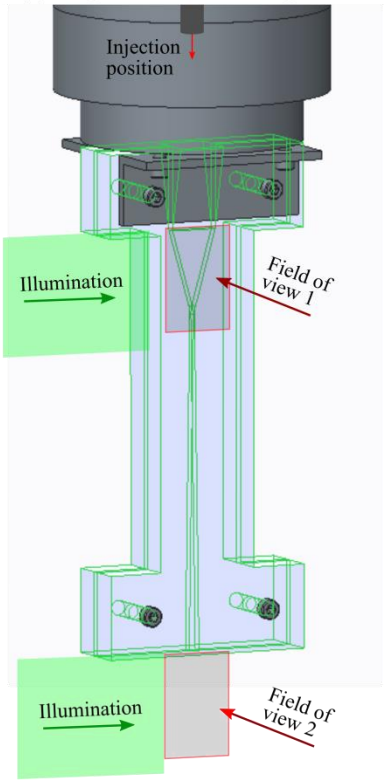

(c) Quartz Nozzle

Fig. 1. a) Scheme of experimental set-up ,b) picture of the measurement system in the laboratory, c) illustration of transparent quartz nozzle.

Secondly, the measurement area just downstream of the nozzle exit, downstream to 50mm standoff distance was analysed in order to have a more complete picture of the outcome of the internal effects. The nozzle sprayed into the measurement section of an enclosed area, which ensured undisturbed flow in absence of a substrate.

Feedstock	Stellite-21			8440 kg/m^3
Stagnation temperature	293K			
Pressures at nozzle inlet	3.4	5.1	6.2	8.0
Powder feeder wheel speeds	5%	10%	15%	20%
Locations of measurement	Converging section			Jet (nozzle exit)

Table 1. Parameter and spray conditions.

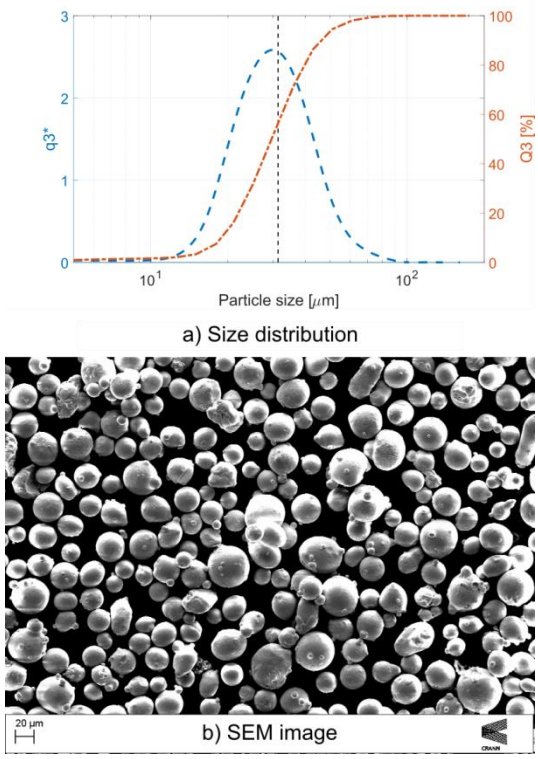

Fig. 2. Measured CS powder, Stellite-21: a) size distribution, b) SEM image.

Fig. 2 shows details of the used powder Stellite-21, a cobalt–chrome alloy. It was used as the spray material representing a relevant material in CS applications, and mostly because it offers advantages both for the injection stability and the optical imaging behaviour inside and outside the nozzle. For the measurement technique, it is essential to gather images at well-defined flow and feeding conditions, such that a stable, continuous flow is even more critical than during the coating application process. Moreover, the illumination as described below depends on the particle size and shape, as well as the reflectivity of the surface. Stellite-21 is a favourable candidate in this respect. As can be seen in **Fig. 2**, it has a standard size distribution between 10 to 60 µm at a Volumetric Mean Diameter (VMD) is approximately 30 µm and a nice spherical particle structure.

2.2 Measurement set-up and testing

Particle Tracking Velocimetry was used to optically measure the particle velocity within the jet. They were illuminated with two subsequent laser pulses formed to a light sheet in the plane of measurement. A camera system captured two images of the scattered light respectively with varying pulse separation time depending on the conditions. These images were processed by a cross–correlation algorithm, deducing the particle displacement, which corresponds to velocity information by knowledge of the pulse separation. A Nd:YAG Laser with a wavelength of 532nm and 6ns pulse duration was used as the light source at 4Hz repetition rate. The pulse separation time was adjusted between 1 and 5µs depending on the velocity level, aiming for an approximate displacement of 10px, allowing for a prolonged dynamic range towards the lower end. The light sheet was formed by a telescope of spherical lenses for the sheet thickness of approximately 1mm and a cylindrical lens for the sheet width of 60mm respectively, illuminating the plane of symmetry in and downstream of the nozzle. A monochromic camera with a resolution of 1280x1024 pixels of 6.7µm pixel size delivered the consecutive image pairs The camera lens aperture was set to f/8.0 in order to minimise lens aberrations. The observed particle image size was found between 2 and 5px. The depth of field was approximately 9mm accordingly. The pre–processing of images included a standard background subtraction of an averaged image from 100 samples in absence of particles and high–pass filtering of the raw data to reduce stationary image features and low–frequency background variations with a kernel width of 5px. The image processing involved a two-step approach, in which a PIV step was used as a predictor for the PTV algorithm, identifying single particle vectors. Along with the hardware, the algorithms were produced by *LaVision* as part of *DaVis v7.2*.

A multitude of sources contributes to the measurement error in PIV and PTV, of which the most important are optical uncertainties (e.g. lens aberrations and calibration errors) and algorithm-related errors (rms displacement error and a bias or “peak-locking” error). From target plane images, we estimate a maximal calibration uncertainty of 0.03px for a 10px displacement. Based on the primary peak ratio in the correlation plane of the measurement images, the rms error could be estimated in the order of 1.3%. This value was conservatively corrected according to previous thorough analysis of the algorithm [28], which results in an rms error of 0.18px or 1.8% on the average displacement. Lastly, the used algorithm for particle tracking was shown to have exceptionally low bias error [28], hence this source

was not considered further. In addition, repeatability of the test cases was assured and the respective standard deviation, as well as the deduced PIV errors were included in the reported errors bars of the measurements given in sections to follow.

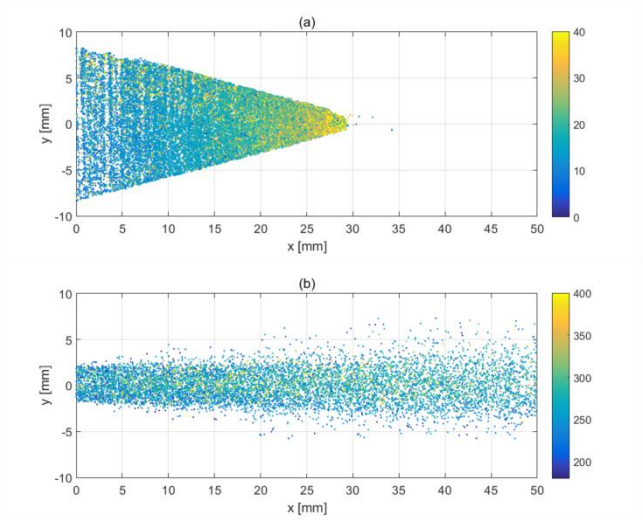

Fig. 3. Scatter plots of particle velocity at 8bar and 140gmin^{-1} (a) in the converging section of nozzle and (b) in the jet.

3 Results and Discussion

3.1 Particle distribution and velocity profile

In order to compare the phase-coupling effect, it is useful to start by exploring the particle velocity distribution under varying conditions. **Fig. 3** shows a comparison of the particle distributions at 8bar in the planes of measurement (a) for the converging section of the nozzle and (b) for the jet downstream of the exit, coloured by the velocity magnitude. This illustration gives a good impression of the velocity change within the nozzle just upstream of the nozzle restriction. Measurement of the velocity further downstream within the nozzle was not feasible due significant change of the optical properties of the quartz surfaces. While the particles on average accelerate up to 30-40m/s, individual particles are much faster than the average throughout almost all the field. At the nozzle exit, the particle velocity spans between 200 and 400m/s. It does not change significantly in the streamwise direction in the jet. As expected, the strongest acceleration must occur just downstream of the nozzle throat. Nevertheless, the observed internal region offers clues about the condition of particles in the more dense region just upstream of this point. It is plausible to say, that during the peak acceleration in the diverging section, effects of interaction between particles drasticly reduce due to their increasingly large average distance.

A comparison of the axial velocity distribution within this dense flow region is shown in **Fig. 4**, comprising results at (a) 3.4 and (b) 8.0bar, each at the lowest and highest feeder wheel speed setting. Each data point represents a moving average including whiskers for the standard deviation of the velocity values. Interestingly, the average velocity at low pressures is almost very similar for both loadings. The statistical distribution is, however, somewhat wider, which suggests that the higher loading results in a stronger mixing and a more unordered flow. At higher pressures, this effect is aggravated drastically, which can be seen by the much larger standard deviation for the high feed rate. More momentum within the flow results in an increase of particle-particle interactions. In fact, the particle velocities are sufficiently more randomly enhanced, that the average velocity lies above the low loading case. At the same time, the axial profile flattens slightly, since the random motion is strong throughout the converging section. It should be mentioned that the study also showed up to a 5-fold increase in the standard deviation of the particle trajectory orientation.

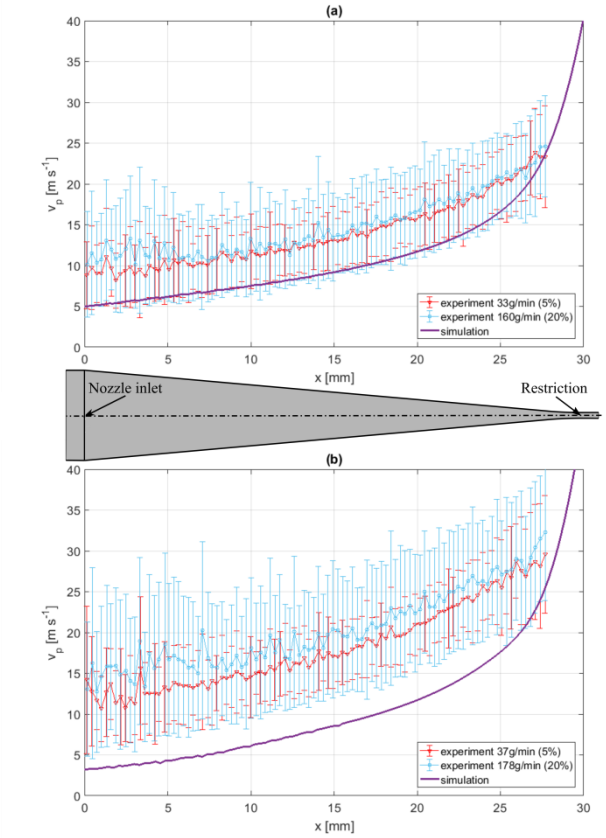

Fig. 4. Axial particle velocity distribution in converging section for (a) 3.4bar and (b) 8.0bar at 5% and 20% feeder wheel speed (ca. 30 and 170g/min), compared to simulation data.

The figure also shows the average velocity profile of particles from a computational model. Fluent v16.0 was employed to model the gas phase in a 3D-steady-state RANS with a realizable k-ε-turbulence model. A density-based solver in an implicit formulation along with a ROE-FDS flux splitting and second-order upwind schemes was used as the discretization method. The particle model is a Lagrangian discrete phase model, which computes the particle trajectory based on a high-Mach number drag law, and accounts for the particle size distribution. This model delivers signifiacantly lower

particle velocities than measured, while the rate of increase is in fairly good agreement. It does not account for particle-particle interactions or the volume fraction, which gives an explanation for the mismatch.

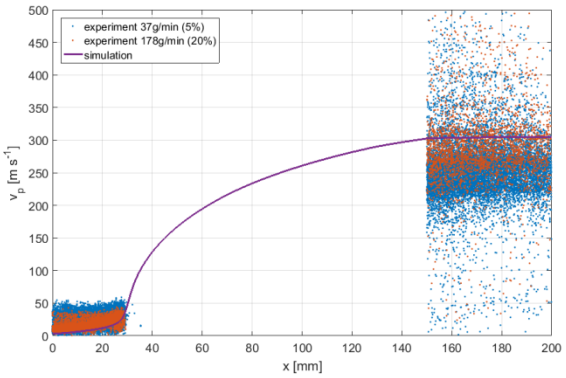

Fig. 5. Axial particle velocity profile at 8bar (experimental and CFD) and increasing particle feed rate.

Conclusively, particle motion within the low-velocity section of the nozzle significantly depends on the particle packing density and is characterised not only by gas particle, but also by particle-particle interactions. This makes the process dependant on both volume and mass fraction of the discrete phase. Downstream of the internal measurement section, the gas expansion leads to a rapid particle acceleration, that increases the average distance between particles. In the diverging section, the primary force on particles is therefore the drag force. In **Fig. 5** the regions 0-30mm and 150-200mm are populated with velocity PTV data points; for comparison a simulation curve is superimposed and also covers the 30-150mm region where there is no experimental data. The figure presents the 8bar case, demonstrating clearly that the increasing feed rate reduces the final velocity level, despite a higher velocity in the throat (by PTV results). The reason lies in the losses that characterise the phase interactions and is discussed below. A comparison of the simulation and experiment shows an underestimation of the mean particle trend in the converging part and an overestimation of the velocity level in the jet. As a sidenote, it should be mentioned that, since the particle velocity upon impact is cruicial for the resulting coating in a process, the simulation tool is not a conservative approach for process design.

3.1 Velocity trends and loading mechanisms

On average, the particle velocity increases in the converging section due to random, collision-driven motion, and decreases as a result of the energy and momentum lost from the gas phase. Hence, the particle behaviour at the inlet and outlet regions of the nozzle is opposite. **Fig. 6** quantifies this connection in a comparison of the mean velocity developments in (a) the converging section and (b) the jet for the different measured pressure levels in dependence of the particle mass loading Z (the fraction of particle mass and gas mass flux), which characterises the momentum exchange between phases according to previous findings [26]. As expected, the overall velocity level increases with pressure throughout the field. As noted above, it can be seen again that the average velocity increases with mass loading in the converging section, and the reverse is true in the jet. Most importantly, the gradients of the shown regression lines differ depending on the pressure. If these gradients are normalised by each velocity level, in order to make a comparison meaningful, we can investigate the susceptibility of the material to mass loading. The same can be done for the volume fraction F (the fraction of particle and an estimated gas volume flux, here with reference to conditions in the restriction). These normalised gradients are denoted $Gr_{Z,n}$ and $Gr_{F,n}$ and represented in **Fig. 7**.

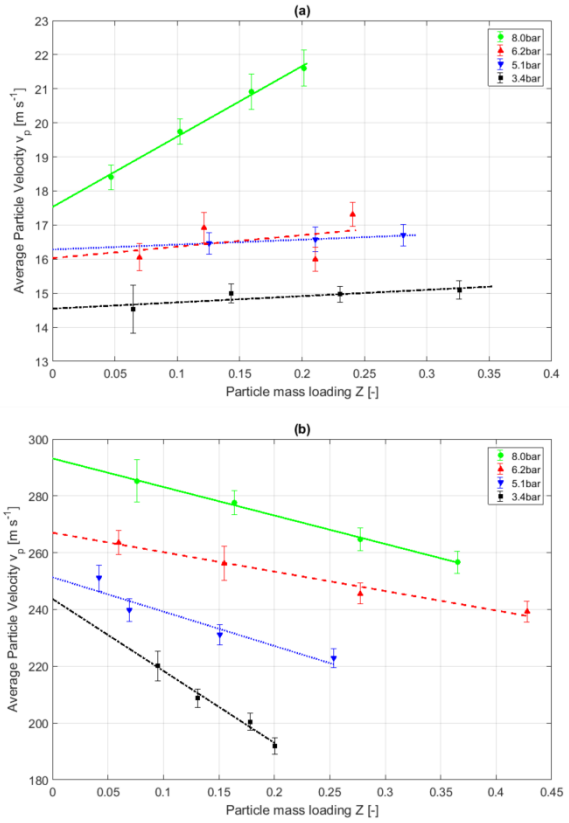

Fig. 6. Average particle velocity change over pressure and particle mass loading in (a) converging section and (b) in the jet.

Focusing on the gradient with mass loading $Gr_{Z,n}$, it should be explained first that the positive gradients for the converging section represent a gain in particle momentum as an outcome of strong mixing, particle collisions and a resulting randomised motion. At low pressures, this gradient is small, as the collisional rate is still low. With higher pressure, more momentum (and hence energy) is gained by particles as collisions become stronger. The negative gradients represent the jet behaviour and stand for a loss of particle momentum (and energy) due to mass loading. At low pressures, this effect is strong, as a the gas flux is rather weak and a unit increment of mass loading can

withdraw a significant protion of energy from the gas flux during the acceleration in the nozzle. At higher pressures, the gas flow is much more energetic, and consequently, a smaller part of this access momentum flux is transferred to the particle phase. At the same time, despite stronger collisional losses in the dense flow region, the stronger velocity increase at higher pressure also goes hand in hand with a smaller loss of velocity in the jet, which makes these opposing trends very plausible.

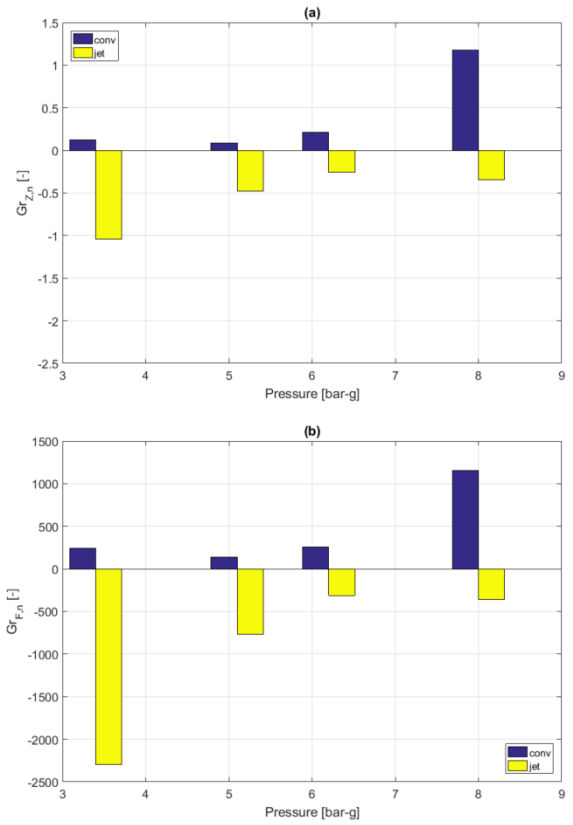

Fig. 7. Pressure dependencte of particle velocity change with (a) mass loading and (b) volume fraction.

Fig. 7b) displays the gradients of same velocity drop with respect to volume fraction. Although the trends remain the same as explained above, the relative change of the magnitude of the gradients has interesting implications. The difference between mass and volume parameters Z and F mainly goes back to the gas density. While the mass is important for the momentum exchange, the volume fraction is directly connected to the displacement of fluid and the geometric distance of particles. This means a high volume fraction can play an important role in the dense flow region. Comparing the two subfigures, we can see that the density significantly scales up the low-pressure gradients with respect to the high-pressure gradients. In a volume fraction-driven loss mechanism, one would expect that a unit increment of volume fraction produces a similar increment of loss or gain for all pressure levels. In other words, in such a mechanism, it should not be gas density-dependent how much engery and momentum is exchanged between phases. In this case, however, particularly in the jet, the low pressure increments of losses are more strongly dependent on volume fraction than on mass loading which suggests that density plays a significant role. This implies that the observed effects are overall predominantly momentum-driven. This is particularly creditable under the consideration a high density material. On the other hand, an increasing dependency could be inferred for the higher pressure, where the trend in the jet begins to reverse and the gradient with respect to volume fraction remains almost constant over a large pressure change. In combination with the strongest enhancement of the particle dynamics in this region, the rising importance of the volume fraction appears logical.

4 Conclusions

The acceleration of particles and the potential causes for coupling effects in Cold Spray primarily take place within the nozzle, while the optical measurements of particle velocity to date had to be conducted downstream of its exit. This limitation to the outcome of the acceleration was firstly overcome in the present study in order to start understanding the driving mechanisms for complex particle-gas interactions. Therefore, this work investigated the particle velocity within the converging section of a 10-bar quartz nozzle and in the free jet. PTV was employed to measure Stellite-21 particle velocities at varying low stagnation pressures and increasing feeding conditions. The study presented an increasing tendency to random motion in the converging section due to higher feed, connected to particle collisions, which is strongly aggravated for higher pressures. Nevertheless, the velocity in the jet decreases with increasing loading as more momentum is withdrawn from the gas phase during the overall particle flight. Because of the stronger momentum flux and the higher momentum particles emerging from the low-speed section, the average drop in the jet is weaker for high pressures. An investigation of the strength of the velocity drops with loading and volume fraction was presented as a susceptibility analysis. In this, it was found that the overall interaction is rather momentum-driven at low-pressure scenarios, whereas the high-pressure case becomes more influenced by the volume fraction, in connection with the strong nozzle-internal particle collisions.
Future investigations are required to extend the region of measurement, as a portion of the nozzle flow still remains implicit.
This study presented the very first attempt to measure particle motion within a CS nozzle. This novelty can be further developed and herein offers opportunities to study the character of particle acceleration and, moreover, enables direct observations of the injection process.

Acknowledgements
The authors wish to express their gratitude to FP7 Marie Curie Actions (Grant 333663) for the financial support.

5 Literature

[1] A. Alkhimov, V. F. Kosarev, and A. Papyrin, “Method of Cold-Gas Dynamic Spraying,” *Dokl. Acad. Nauk SSSR*, vol. 315, no. 5, pp. 1062–1065, 1990.

[2] A. Papyrin, “COLD SPRAY TECHNOLOGY,” *Adv. Mater. Process.*, vol. 159, no. 9, pp. 49–51, 2001.

[3] H. Assadi, F. Gärtner, T. Stoltenhoff, and H. Kreye, “Bonding mechanism in cold gas spraying,” *Acta Mater.*, vol. 51, no. 15, pp. 4379–4394, 2003.

[4] M. Grujicic, C. L. Zhao, C. Tong, W. S. DeRosset, and D. Helfritch, “Analysis of the impact velocity of powder particles in the cold-gas dynamic-spray process,” *Mater. Sci. Eng.*, vol. 368, no. 1–2, pp. 222–230, 2004.

[5] T. Han, Z. Zhao, B. a. Gillispie, and J. R. Smith, “Effects of Spray Conditions on Coating Formation by the Kinetic Spray Process,” *J. Therm. Spray Technol.*, vol. 14, no. 3, pp. 373–383, 2005.

[6] E. H. Kwon, S. H. Cho, J. W. Han, C. H. Lee, and H. J. Kim, “Particle behavior in supersonic flow during the cold spray process,” *Met. Mater. Int.*, vol. 11, no. 5, pp. 377–381, 2005.

[7] T. C. Jen, L. Li, W. Cui, Q. Chen, and X. Zhang, “Numerical investigations on cold gas dynamic spray process with nano- and microsize particles,” *Int. J. Heat Mass Transf.*, vol. 48, no. 21–22, pp. 4384–4396, 2005.

[8] H. Katanoda, T. Matsuoka, and K. Matsuo, “Experimental study on shock wave structures in constant-area passage of cold spray nozzle,” *J. Therm. Sci.*, vol. 16, no. 1, pp. 40–45, 2007.

[9] S. Yin, Q. Liu, H. Liao, and X.-F. Wang, “Effect of injection pressure on particle acceleration, dispersion and deposition in cold spray,” *Comput. Mater. Sci.*, vol. 90, pp. 7–15, Jul. 2014.

[10] S. Yin, X. Suo, H. Liao, Z. Guo, and X. Wang, “Significant influence of carrier gas temperature during the cold spray process,” *Surf. Eng.*, vol. 30, no. 6, pp. 443–451, 2014.

[11] F. Gärtner, T. Stoltenhoff, T. Schmidt, and H. Kreye, “The Cold Spray Process and Its Potential for Industrial Applications,” *J. Therm. Spray Technol.*, vol. 15, no. 2, pp. 223–232, 2006.

[12] A. Sova, A. Okunkova, S. Grigoriev, and I. Smurov, “Velocity of the Particles Accelerated by a Cold Spray Micronozzle: Experimental Measurements and Numerical Simulation,” *J. Therm. Spray Technol.*, vol. 22, no. 1, pp. 75–80, Nov. 2012.

[13] S. Li, B. Muddle, M. Jahedi, and J. Soria, “A Numerical Investigation of the Cold Spray Process Using Underexpanded and Overexpanded Jets,” *J. Therm. Spray Technol.*, vol. 21, no. 1, pp. 108–120, Oct. 2011.

[14] X.-F. Wang, S. Yin, and B. P. Xu, “Effect of cold spray particle conditions and optimal standoff distance on impact velocity,” *J. Dalian Univ. Technol.*, vol. 51, no. 4, pp. 498–504, 2011.

[15] W.-Y. Li and C.-J. Li, “Optimization of spray conditions in cold spraying based on numerical analysis of particle velocity,” *Trans. Nonferrous Met. Soc. China (English Ed.*, vol. 14, no. 2, pp. 43–48, 2004.

[16] D. L. Gilmore, R. C. Dykhuizen, R. A. Neiser, T. J. Roemer, and M. F. Smith, “Particle Velocity and Deposition Efficiency in the Cold Spray Process,” *J. Therm. Spray Technol.*, vol. 8, no. 4, pp. 576–582, 1999.

[17] H. Fukanuma, N. Ohno, B. Sun, and R. Huang, “In-flight particle velocity measurements with DPV-2000 in cold spray,” *Surf. Coatings Technol.*, vol. 201, no. 5, pp. 1935–1941, 2006.

[18] B. Jodoin, F. Raletz, and M. Vardelle, “Cold spray modeling and validation using an optical diagnostic method,” *Surf. Coatings Technol.*, vol. 200, no. 14–15, pp. 4424–4432, 2006.

[19] F. Raletz, M. Vardelle, and G. Ezo’o, “Critical particle velocity under cold spray conditions,” *Surf. Coatings Technol.*, vol. 201, no. 5, pp. 1942–1947, 2006.

[20] X.-J. Ning, Q.-S. Wang, Z. Ma, and H.-J. Kim, “Numerical Study of In-flight Particle Parameters in Low-Pressure Cold Spray Process,” *J. Therm. Spray Technol.*, vol. 19, no. 6, pp. 1211–1217, Sep. 2010.

[21] S. P. Pardhasaradhi, V. Venkatachalapathy, S. V Joshi, and S. Govindan, “Optical Diagnostics Study of Gas Particle Transport Phenomena in Cold Gas Dynamic Spraying and Comparison with Model Predictions,” *J. Therm. Spray Technol.*, vol. 17, no. 4, pp. 551–563, Oct. 2008.

[22] B. Samareh, O. Stier, V. Lüthen, and A. Dolatabadi, “Assessment of CFD Modeling via Flow Visualization in Cold Spray Process,” *J. Therm. Spray Technol.*, vol. 18, no. 5–6, pp. 934–943, Aug. 2009.

[23] R. Lupoi, “Current design and performance of cold spray nozzles: experimental and numerical observations on deposition efficiency and particle velocity,” *Surf. Eng.*, vol. 30, no. 5, pp. 316–322, Jun. 2014.

[24] M. Meyer and R. Lupoi, “An analysis of the particulate flow in cold spray nozzles,” *Mech. Sci.*, vol. 6, no. 2, pp. 127–136, 2015.

[25] M. Meyer, S. Yin, K. A. Mcdonnell, O. Stier, and R. Lupoi, “Feed rate effect on particulate acceleration in Cold Spray under low stagnation pressure conditions,” *Surf. Coatings Technol.*, vol. 304, pp. 237–245, 2016.

[26] M. Meyer, S. Yin, and R. Lupoi, “Particle in-flight velocity and dispersion measurements at increasing particle feed rates in Cold Spray,” *J. Therm. Spray Technol.*, vol. 16, no. 1–2, pp. 60–70, 2017.

[27] O. Stier, “Fundamental cost analysis of cold spray,” *J. Therm. Spray Technol.*, vol. 23, no. 1–2, pp. 131–139, 2014.

[28] M. Stanislas, K. Okamoto, C. J. Kähler, and J. Westerweel, “Main results of the Second International PIV Challenge,” *Exp. Fluids*, vol. 39, no. 2, pp. 170–191, 2005.